DOI 10.1007/s11204-022-09804-9
Soil Mechanics and Foundation Engineering, Vol. 59, No. 3, July, 2022 (Russian Original No. 3, May-June, 2022)

SOIL MECHANICS

NONLINEAR ELASTIC-PERFECTLY PLASTIC MODEL OF SOIL AND ITS NUMERICAL IMPLEMENTATION AND APPLICATION

UDC 624.131.5/531

X. Xu,[1] Z.-H. Dai,[2]* L.-J. Chen,[2] and X.-T. Xu[1]

[1]Fujian Agriculture and Forestry University, Fuzhou, China; [2]Fuzhou University, Fuzhou, China,
*Corresponding author E-mail: dzhang@fzu.edu.cn.

To combine the advantages of the Mohr-Coulomb and the Duncan-Chang models, a new model called the nonlinear elastic-perfectly plastic model was established. In the numerical implementation of this model, a newly developed smoothing technique for yield and plastic potential surfaces was employed to accurately fit the side face of the hexagonal pyramid surface of the Mohr-Coulomb criterion. A user material subroutine was developed in Abaqus and was verified by modeling a conventional triaxial test of a soil specimen with the feature of a nonlinear elastic-perfectly plastic model. Finally, to further validate the applicability of this model and its subroutine, the 3D numerical simulation of a relatively complex deep excavation project was performed, and the results were compared with measured data, the results determined by the method recommended in the current code, and the results of the Mohr-Coulomb and Duncan-Chang models. The comparison demonstrates that the results of this new model were the closest to the measurements.

Introduction

Numerous experiments have shown that the Mohr-Coulomb (M-C) yield criterion can reasonably predict the yielding or failure of soil and rock. However, as is generally known, the M-C yield criterion represents a hexagonal pyramid surface in three-dimensional principal stresses space, which limits numerical computation due to the gradient discontinuities that occur at both the edges and the tip of the hexagonal pyramid surface. Many researchers have proposed various methods to solve these difficulties [1-3]. In particular, Abbo and Sloan [2] presented a simple hyperbolic yield surface to eliminate the singularity of the M-C surface. Later, a practical subroutine based on their methodology was developed by Jia et al. [4]. These studies have greatly promoted the development of techniques to address the numerical singularity of the M-C criterion so that the simple linear elastic-perfectly plastic model could be widely employed in the numerical analysis of geotechnical engineering. However, the M-C model is more reliable for stability analysis than for deformation analysis in geotechnical engineering applications. As is generally known, no constitutive relation of any soil coincides with the M-C model because no soil fully obeys linear elastic behavior before yielding. As a result, the M-C model is unable to accurately predict the deformations of soils under various loading and/or unloading cases.

Usually, the stress-strain relationship of soil is nonlinear, even if subjected to a small load. In this respect, the Duncan-Chang (D-C) model can reasonably reflect the nonlinear elastic properties of hardening soil [5]. In this model, an unloading or reloading deformation modulus E_{ur} is introduced to discriminate it from the monotonic loading modulus E_t to reflect unrecoverable residual deformation, which can be considered as plastic deformation. For this reason, the D-C model can be applied to numerical computations not only in loading cases but also in unloading or reloading cases such as in excavation engineering [6]. Nevertheless, the D-C model is not able to take yielding or softening into account.

As mentioned above, the prevailing M-C and D-C models have unique advantages and disadvantages. To combine the advantages and overcome the disadvantages of these two models, a new constitutive model called the nonlinear elastic-perfectly plastic model was established, in which the D-C model and M-C yield criterion are used to describe the nonlinear elastic-perfectly plastic stress-strain relationship before and after yielding, respectively. Theoretically, this new model can exactly or approximately match the experimental curves of some soils that exactly or approximately exhibit these

Translated from Osnovaniya, Fundamenty i Mekhanika Gruntov, No. 3, May-June, 2022.
0038-0741/22/5903-0215 © 2022 Springer Science+Business Media, LLC

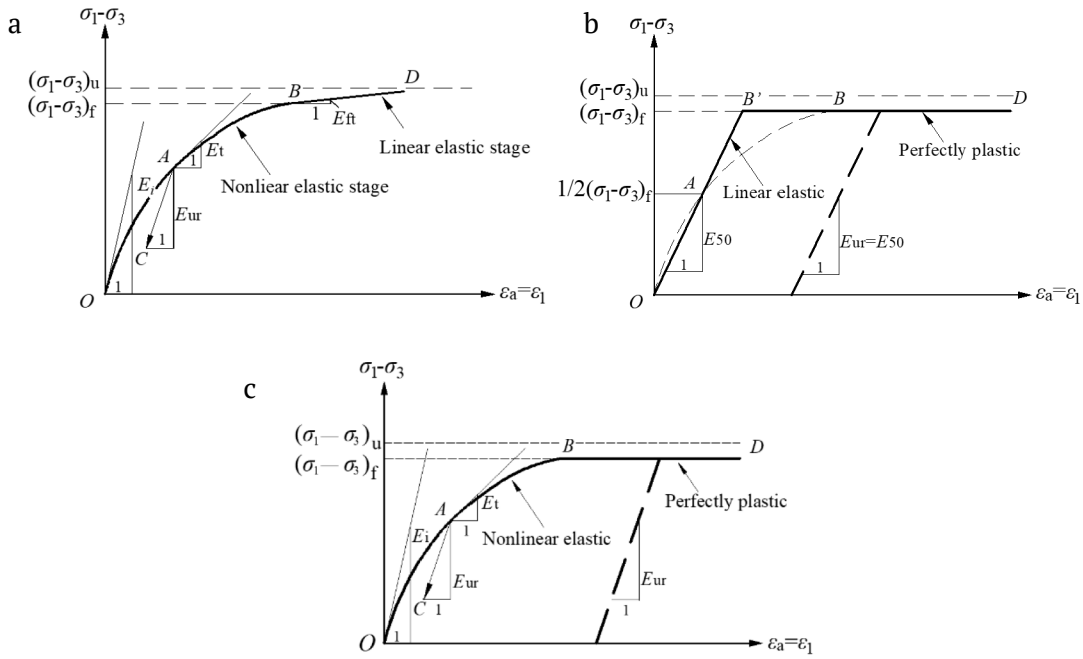

Fig. 1. Stress-strain relationships: a) D-C model, b) M-C model, and c) new model.

features. For the convenience of application, a FORTRAN subroutine was successfully developed for this model in the secondary development interface of the finite element software Abaqus, and this subroutine will be verified by numerically modeling the triaxial test of a soil specimen. Furthermore, this subroutine will be applied in the 3D numerical analysis of a deep excavation project.

Establishment of Nonlinear Elastic-Perfectly Plastic Model of Soil

A schematic diagram of the D-C nonlinear elastic model is illustrated in Fig. 1a. The M-C model is plotted in Fig. 1b, and usually, the secant elastic modulus $E_{50,}$ which corresponds to half (50%) of the deviatoric stress at failure, is taken as the elastic modulus of the soil for both the loading and unloading cases. A schematic diagram of the new model, which is the integration of the D-C and M-C models, is shown in Fig. 1c. In the existing D-C model, there is only a fuzzy judgment condition indicating that the soil fails if the tangent modulus approaches zero, but this modulus cannot decrease to zero; therefore, a lower bound of the tangent modulus $E_{t\min}$ (which will be introduced later) is set [7]. Hence, there is no clear concept of plastic yielding and judgment in the D-C constitutive model, but this can be included using the M-C model. That is, in this new model, the horizontal line *BD* of the M-C model will be employed to replace the oblique line *BD* of the D-C model.

Nonlinear elastic stage. As shown in Fig. 1, the nonlinear elastic stage is indicated by segment *OB*, in which the relationship of $(\sigma_1 - \sigma_3)$ vs ε_1 can be expressed as a hyperbola, taking $(\sigma_1 - \sigma_3) = (\sigma_1 - \sigma_3)_u$ as its asymptote, where $(\sigma_1 - \sigma_3)$ is the deviatoric stress and ε_1 is the major (axial) principal strain. In Fig. 1, E_i and E_t are the initial tangent modulus and the tangent modulus at any deviatoric stress, respectively; $(\sigma_1 - \sigma_3)_f$ is the deviatoric stress at failure, and all these parameters can be determined (refer to [5] for details).

The value of E_t decreases with increasing deviatoric stress. To prevent the tendency of the model to underestimate the lateral stresses in the soil elements with a small confining stress and a low stress level and to avoid the presence of tension stresses, Seed and Duncan [7] set a lower bound for E_t, i.e.,

$$E_{t\min} = 0.25KP_a(0.02)^n, \quad (1)$$

where K and n are the experimental constants, P_a is the atmospheric pressure.

Perfectly plastic stage. In incremental analyses, once the stress level $S_1 = (\sigma_1 - \sigma_3)/(\sigma_1 - \sigma_3)_f$ is greater than or equal to 1.0, or in other words, once the M-C criterion

$$F = (\sigma_1 - \sigma_3) + (\sigma_1 + \sigma_3)\sin\phi - 2c\cos\phi = 0 \tag{2}$$

is met (where c and ϕ are the effective cohesion and angle of internal friction of the soil, respectively), the perfectly plastic stage will be reached, as indicated by segment *BD* shown in Figs. 1b and 1c.

As is well known, the gradient discontinuities that occur at both the edges and the tip of the hexagonal pyramid surface will bring about numerical singularity, leading to the inefficiency or failure of stress integration schemes. To avoid this problem, the embedded M-C model in Abaqus employs the plastic potential function, *G*, proposed by Menétrey and William [8], which is inconsistent with the yield function *F* of the M-C criterion. Since there exists a difference in shape between the potential and yield surfaces, the flow rule is always non-associated in the embedded M-C model, and errors in the plastic strains or deformations must exist. To replicate the M-C surface and allow both the associated and non-associated flow rules to be implemented in Abaqus, this work adopts the hyperbolic yield function proposed in [2], which is rounded in both the meridional and deviatoric planes. The relevant mathematical expressions are

$$F = \sigma_m \sin\phi + \sqrt{\bar{\sigma}^2 K^2(\theta) + a^2 c^2 \sin^2\phi} - c\cos\phi = 0, \tag{3}$$

$$K(\theta) = \begin{cases} A - B\sin 3\theta & |\theta| > \theta_T \\ \cos\theta - \dfrac{1}{\sqrt{3}}\sin\phi\sin\theta & |\theta| \le \theta_T \end{cases}, \tag{4}$$

$$A = \frac{1}{3}\cos\theta_T \left[3 + \tan\theta_T \tan 3\theta_T + \frac{1}{\sqrt{3}} sign(\theta)(\tan 3\theta_T - 3\tan\theta_T)\sin\phi \right], \tag{5}$$

$$B = \frac{1}{3\cos 3\theta_T}\left(sign(\theta)\sin\theta_T + \frac{1}{\sqrt{3}}\cos\theta_T \sin\phi \right), \tag{6}$$

$$sign(\theta) = \begin{cases} +1 & \theta \ge 0^\circ \\ -1 & \theta < 0^\circ \end{cases}, \tag{7}$$

where $sign(\theta)$ is the sign function, θ_T is the transition angle (θ_T ranges from 0° to 30°), and the greater θ_T is, the better the fitting to the M-C cross-section in the deviatoric plane. However, θ_T should not be too close to 30° in order to avoid the ill-condition, and Abbo and Sloan [2] recommended its maximum to be 25°. Although this paper set θ_T = 29°, which was consistent with the value suggested by Owen and Hinton [9], computations can still converge rapidly. In addition, the negative branch of the hyperbola was chosen to consider the tensile strength of soil through parameter *a*.

Equation (3) can approach the M-C yield function as closely as desired by adjusting parameter *a* and may degrade to the M-C yield function if *a* = 0 (see Fig. 2). When *a* = 0.05 and θ_T = 25°, the hyperbolic surface approaches the M-C yield surface with a maximum difference of less than 0.15% [2]. Better results were obtained by letting θ_T = 29° rather than 25° in this work to further approach the edges of the hexagonal pyramid surface of the M-C criterion.

A plastic potential function *G* similar to the hyperbolic yield function *F* (see Eq. (3)) is employed. The only difference is that the angle of internal friction of soil ϕ is replaced by the dilation angle ψ ($\psi \leqslant \phi$). If $\psi = \phi$, the associated flow rule is adopted; otherwise, the non-associated flow rule is used. The discrepancy of the potential surfaces between the new model and the embedded M-C model is shown in Fig. 3. In theory, the plastic strain computed by the former will be more reasonable than that of the latter because its potential surface agrees with the true M-C yield surface much better than that of the latter.

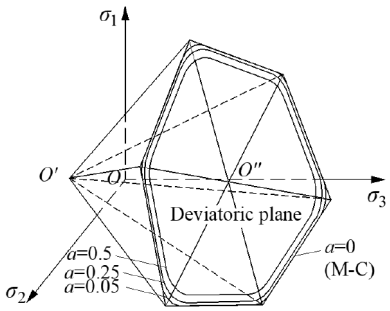

Fig. 2. M-C yield surface in the 3D principal stress space and Abbo's rounded yield surface in the deviatoric plane.

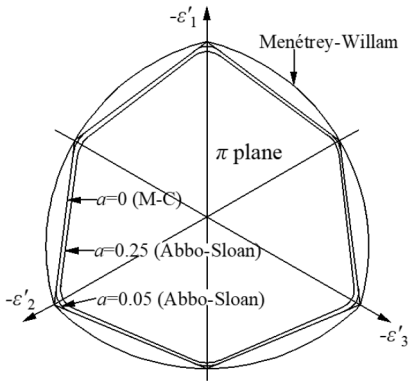

Fig. 3. Comparisons of potential surfaces in the π plane with the projections of three principal strain axes.

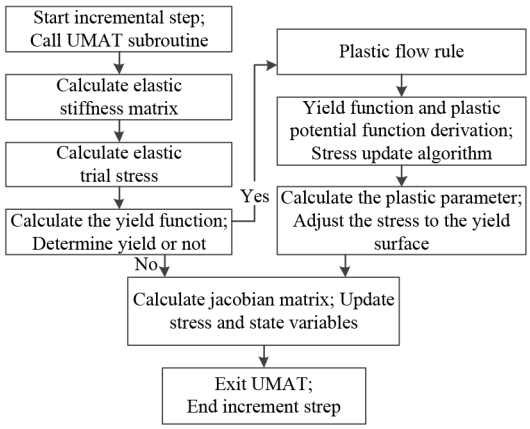

Fig. 4. Flow chart for calling the UMAT and numerical algorithms.

A subroutine of the user material model (UMAT) based on the new model was developed in Abaqus (Fig. 4). In the process of loading, the trial stresses of the Gaussian points of some elements may exceed the yield stresses. They must be adjusted to meet the yield criterion, and correspondingly, the plastic strains should be computed. The specific steps of stress adjustment are described in [9].

Subroutine Verification and 3D Numerical Simulations of an Engineering Case

The plan of the deep excavation project of the Fuzhou Sheng-Hui International Building is square with a side length of 53.7 m. There are two stories of basements in this building. The excavation depth is 6.54 m. The geological and calculation profiles and retaining structures are shown in Fig. 5.

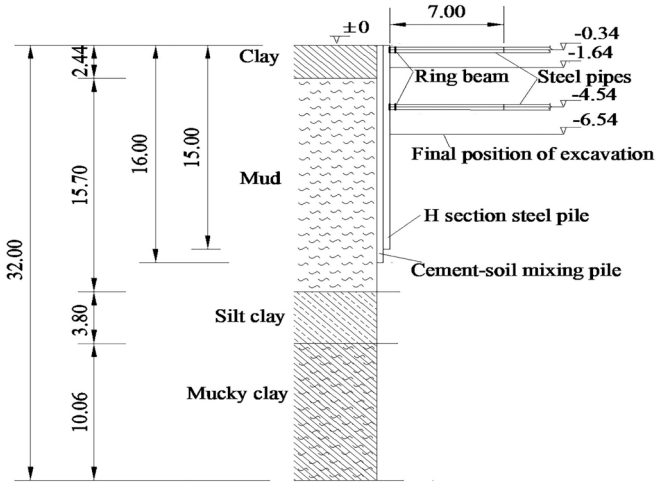

Fig. 5. Typical geological and calculation profile, m.

Steel H-piles with internal supports made with steel pipes and diagonal braces made with steel H-beams were employed to retain the excavation slope, with cement-soil mixing piles serving as a waterproof curtain. Each steel H-pile was 15 m in length, 350 mm in both flange width and cross-section height, and 19 and 12 mm in flange and web thicknesses. The pile spacing (center to center) of two adjacent steel H-piles was 0.8 m. The cement-soil mixing piles were 16 m in length, 0.6 m in diameter, and 0.5 m in pile spacing (center to center). All the steel pipes were 609 mm in outer diameter and 14 mm in wall thickness (Fig. 5). The horizontal spacing between two adjacent steel pipes was 10.7 m, and the vertical spacing between the two rows of steel pipes was 4.2 m. There were two ring beams, each combined with two steel H-beams, to connect the internal supports to the steel H-piles, which was also beneficial to strengthen the stiffness of the entire retaining structure. Each diagonal brace was 8 m long, had the same section dimension as the steel H-piles, and intersected the corresponding steel pipe at an angle of 26.3°. The steel material was Q235, which had a unit weight of 78.5 kN/m^3, an elastic modulus of 2.1×10^8 kPa, and a Poisson's ratio of 0.3. In addition, steel H-beams were employed as support columns and set at each intersection between the longitudinal and transverse steel pipes, but they had no influence on the stiffness of the internal supports; therefore, for the sake of simplicity, they were not modeled. Additionally, the self-weight of all the internal supports was ignored. The cement-soil mixing piles created a diaphragm wall with an elastic modulus of 1.7×10^5 kPa and a Poisson's ratio of 0.3. The design axial prestressing force imposed by the steel pipes in the two rows was 320 kN, and the surcharge of 20 kPa on the ground behind the steel-H piles was taken into account.

The mechanical parameters of the new model are the same as those of the D-C model. In this work, their values were referenced from [6] and listed in Table 1. The parameters were obtained by conventional triaxial compression undrained (CU) and drained (CD) tests in which the K_0 consolidation specimens were adopted to determine the parameters of the D-C model in consideration of the static earth pressure condition during the sedimentary consolidation of the soil mass.

According to the theory of the D-C model, the major principal strains can be calculated by

$$\varepsilon_1 = \frac{\sigma_1 - \sigma_3}{KP_a\left(\frac{\sigma_3}{P_a}\right)^n [1 - R_f S_l]}. \tag{8}$$

To validate the subroutine, a standard cylindrical soil specimen with a diameter of 39.1 mm and a height of 80 mm was modeled and discretized with C3D20R elements (Fig. 6). The bottom of the model

TABLE 1

Soil type	c, kPa	ϕ, °	Duncan-Chang model						Mohr-Coulomb model		
			CU test				CD test				
			R_f	K	n	K_{ur}	K_B	m	E, kPa	ν	ψ, °
Clay	21.43	17.13	0.82	100.53	0.67	217.79	59.90	0.6	2300	0.40	0.1
Mud	12.43	15.07	0.88	108.15	0.67	194.29	62.48	0.32	3670	0.45	0.1
Silt clay	28.80	19.30	0.76	181.92	0.58	318.36	163.84	0.65	200000	0.35	0.1
Mucky clay	22.41	19.96	0.87	162.90	0.57	314.44	100.86	0.49	11960	0.42	0.1

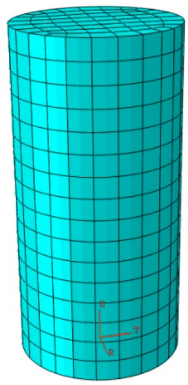

Fig. 6. Finite element model and mesh.

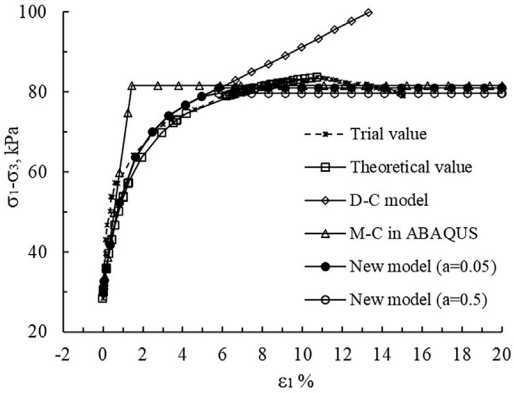

Fig. 7. Comparison of the stress-strain curves from the tests, simulations, and calculations.

was constrained with zero displacement in all directions, and a confining pressure and an axial pressure were applied to the side and top of the model, respectively, to model the K_0 consolidation. Then, the numerical compression test was accomplished by gradually increasing the axial pressure. For example, under the K_0 consolidation (with $\sigma_1 = 100$ and $\sigma_3 = 70$ kPa) and undrained compression test conditions, the mud stress-strain curves determined by the experimentation, theoretical calculation (Eq. (8)) and numerical simulation of the M-C, D-C, and new models are shown in Fig. 7. Notably, some oscillations formed along the backbone curve of the experiment due to the influence of the sensitivity of the triaxial apparatus. When $a = 0.05$, the new model coincided with the D-C model before yielding and the M-C model after yielding. Furthermore, overall, the experimental stress-strain relationship displayed a nonlinear and weak softening behavior that could not be described by either the M-C or D-C model but might be satisfactorily described by the new model. This demonstrates that the new model is accurate and that its subroutine development was successful.

Taking the boundary effect, the characteristics of the simulation object, the geological conditions, and the computational efficiency into account, the size (length × width × height) of the 3D numeri-

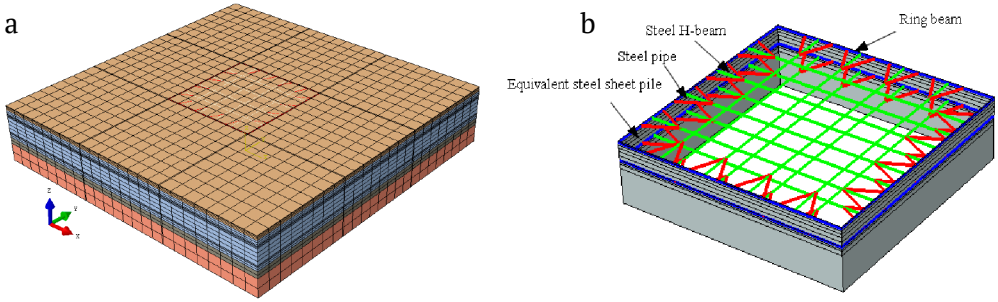

Fig. 8. Finite element models: a) the whole model without excavation, b) retaining structures.

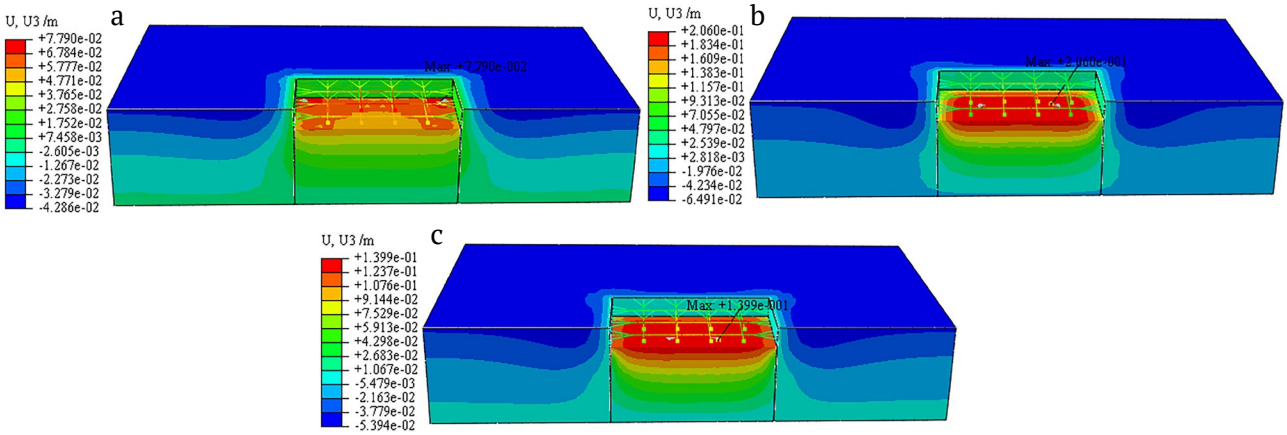

Fig. 9. Contours of vertical displacements: a) D-C model, b) M-C model, and c) new model.

cal model was determined to be 85×85×32 m^3. The overall finite element model before excavation and the model of the retaining structures are shown in Figs. 8a and 8b, respectively. Note that to simplify the finite element model, following the equivalent principle of bending stiffness, each steel H-pile is equivalent to a steel sheet with a rectangular section with a width of 0.8 m (pile spacing) and a height of 0.181 m. Accordingly, the isolated steel H-piles may be regarded as a continuous steel sheet wall with a thickness of 0.181 m (see Fig. 8b) and thus modeled with thick shell elements. The C3D20R, S8R, B32, and T3D2 elements were used to model the soils and diaphragm wall, the equivalent steel sheet piles, the ring beams, the internal supports (steel pipes), and the diagonal braces (steel H-beams), respectively. The round steel pipes and the steel H-beams were modeled according to their true dimensions using the above beam or truss elements.

In practical engineering, excavation and retaining are normally carried out step by step. However, for brevity, only the results of the final construction step are provided here. For example, Fig. 9 shows the contours of the vertical displacements U3 by the D-C, M-C, and new models, respectively. The distribution laws of the vertical displacements were similar, especially those shown in Figs. 9b and 9c. However, the vertical displacement magnitudes were not the same among the different models. The maximum settlement on the ground and the maximum upheaval on the final excavation surface determined by the M-C model were 64.91 and 206.0 mm, respectively; the corresponding values determined by the D-C model were 42.86 and 77.9 mm, respectively; and the corresponding values determined by the new model were between the former two, 53.94 and 139.9 mm, respectively. The differences in these results were attributed to not only the constitutive models but also the parameters, especially the soil moduli, used in each model. In general, the deformations computed by the M-C or D-C model are either overestimations or underestimations due to known shortcomings. However, the deformations computed by the new model may be moderate, and the resulting distribution laws are described next.

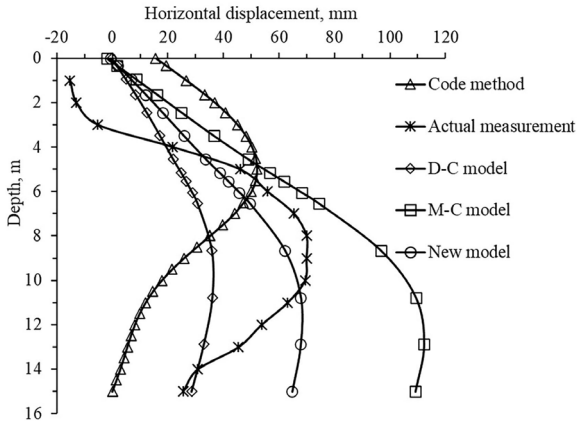

Fig. 10. Comparison of the horizontal displacements of the equivalent steel sheet pile.

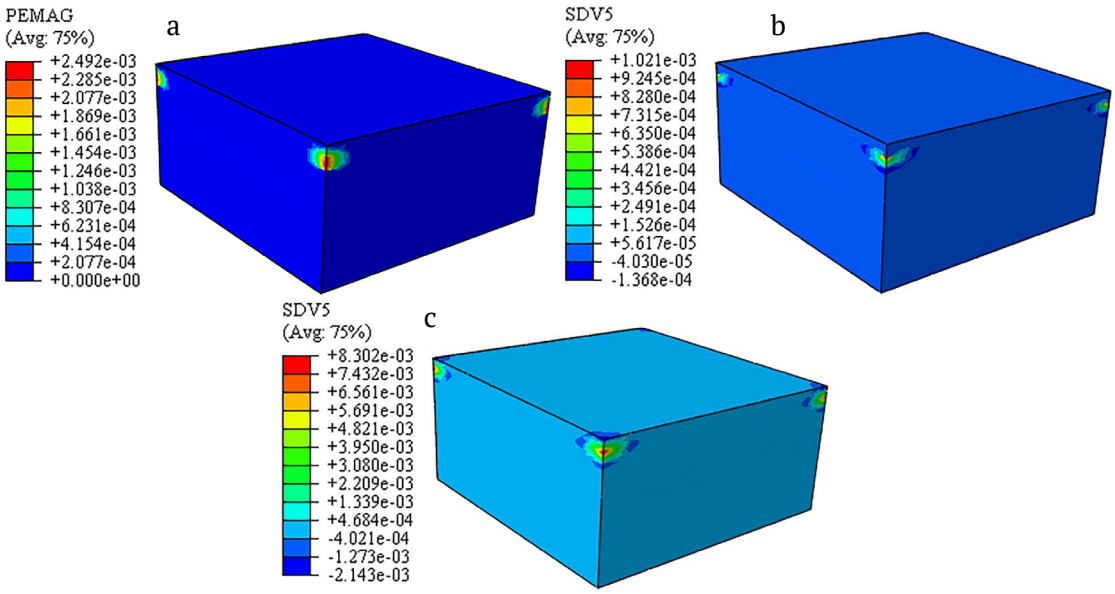

Fig. 11. Contours of equivalent plastic strain in soil: a) M-C model, b) new model with a = 0.05, and c) new model with a = 0.5.

A comparison of the horizontal displacements along the vertical central axis of an equivalent sheet pile wall and the actual measured data and the values calculated by the method recommended in the current code (*m*-method) are provided in Fig. 10. Most likely, overall, the D-C model underestimated the horizontal displacements, which is dangerous, whereas the M-C model overestimated them, which is unnecessarily conservative. However, the position and magnitude of the maximum horizontal displacement determined by the new model were close to those of the measured results. Such prediction results can meet the demands for the design stiffness of retaining structures. Notably, the new model still predicted great differences from the measurements in the upper or lower part. One of the main reasons for this outcome is that the measured data were from an inclinometer installed in the soil near one of the piles close to the central axis, not from the pile itself. In addition, one can see that the results of the upper or lower parts were either greatly overestimated or greatly underestimated by the method recommended in the current code.

Figure 11 shows the contours of the equivalent plastic strains (general plastic strains) in the soil under the final excavation surface by the M-C model and the new model with a = 0.05 and a = 0.5. Clear-

ly, the distribution forms of the former two approaches are quite similar, yet there are great differences in their magnitudes due to the influence of the different plastic potential surfaces shown in Fig. 3. Figure 11c indicates that parameter *a* significantly affects the computed plastic strains. Previous work has shown that the magnitude of *a* may reflect the tensile strength of soil to some extent. Such a plastic zone, of course, cannot be described by the D-C model because the D-C model does not consider plasticity.

Conclusions

A new constitutive model for soils, the nonlinear elastic-ideal plastic model, was presented by combining the Duncan-Chang model with the Mohr-Coulomb elasto-plastic model.

To overcome the numerical singularity and ensure that the new model approaches the hexagonal pyramid surface of the Mohr-Coulomb criterion, near the edges, the yield surface is replaced by the Abbo-Sloan hyperboloid, and the yield and potential functions have similar expressions so that both the associated and non-associated flow laws can be implemented in the new model.

The numerical simulation of a triaxial test shows that the results of the new model fit the measured stress-strain curve fairly well. This proves that the new model can fairly reliably describe soils with a perfect plasticity or weak softening behavior, and that its subroutine is accurate. Another prominent advantage of this new model is that it uses the same parameters as the D-C model, which can be obtained by the conventional triaxial testing that most engineering investigations and design institutes are capable of performing.

The practical application in a deep excavation engineering case shows that among the results of all the methods tested, the results predicted by the new model were the closest to the measured data. Similar to the conventional M-C model, the new model can identify the plastic zone, which is of great significance in the design and analysis of geotechnical engineering, and it can simultaneously consider the nonlinearity before yielding.

Therefore, the new model can be employed to accurately predict not only the ultimate bearing capacity of foundations and the factor of safety of soil slopes but also their deformation before reaching the critical state. Such investigations still need to be performed.

Acknowledgments

The authors gratefully acknowledge the financial support of the National Natural Science Foundation of China (Grant No. 41702288), the Education Department of Fujian Province (Grant No. JAT190138), and the Fujian Agriculture and Forestry University (Grant No. 113/712018R0306). The authors are also grateful to the reviewers for their helpful advice and comments.

References

1. W. T. Koiter, "Stress-strain relations, uniqueness and variational theorems for elastic-plastic materials with a singular yield surface," *Quart. Appl. Math.*, **11**, 350-354(1953).
2. A. J. Abbo and S. W. Sloan, "A smooth hyperbolic approximation to the Mohr-Coulomb yield criterion," *Comput. Struct.*, **54**(3), 427–441(1995).
3. A. J. Abbo, A. V. Lyamin, S. W. Sloan, and J. P. Hambleton, "A C2 continuous approximation to the Mohr–Coulomb yield surface," *Int. J. Solids Struct.*, **48**(21), 3001-3010(2011).
4. S. P. Jia, W. Z. Chen, J. P. Yang, and P. S. Chen, "An elastoplastic constitutive model based on modified Mohr-Coulomb criterion and its numerical implementation (In Chinese)," *Rock Soil Mech.*, **31**(7), 2051-2508(2010).
5. J. M. Duncan and C. Y. Chang, "Nonlinear analysis of stress and strain in soils," *J. Soil Mech. Found. Division*, **96**(5), 1629-1653(1970).
6. L. J. Chen, Z. H. Dai, and Z. W. Liu. "Three-dimensional nonlinear finite element analysis of soft soil excavation engineering considering K0 consolidation (in Chinese)," *Rock Soil Mech.*, **32**(12), 3796-3804(2011).
7. R. B. Seed, and J. M. Duncan, "SSCOMP: A finite element analysis program for evaluation of soil-structure interaction and compaction effects," *Geotechnical Engineering Research Report No. UCB/GT-84-02*, University of California, Berkeley, California. 1984.
8. P. H. Menetrey and K. J. William, "Triaxial failure criterion for concrete and its generalization," *ACI Struct. J.*, **92**(3), 311-318(1995).
9. D. R. J. Owen and E. Hinton, *Finite Elements in Plasticity: Theory and Practice*, Pineridge Press Ltd., Swansea (1980).